POLITECNICO DI TORINO
Repository ISTITUZIONALE

A Comparison of Impedance Eduction Test Rigs with Different Flow Profiles

(Article begins on next page)

01 September 2025

A Comparison of Impedance Eduction Test Rigs with Different Flow Profiles

Lucas A. Bonomo*, Nicolas T. Quintino† and Julio A. Cordioli‡
Federal University of Santa Catarina, Florianópolis - SC, 88040-900, Brazil

Francesco Avallone§
Politecnico di Torino, 10129 Torino, Italy

Michael G. Jones¶, Brian M. Howerton‖ and Douglas M. Nark**
NASA Langley Research Center, Hampton, VA, 23681, USA

The experimental characterization of acoustic liners applied for turbofan engines has been in the spotlight of the community for the last few decades. In general, such characterization is done by measurements of the liner acoustic impedance using different techniques in conditions as close as possible to those encountered in turbofan engines. Although a great amount of work has been published related to these techniques, few comparisons between different experimental setups using identical samples are available. The goal of the present study is to provide a comparison between educed acoustic impedances for two nominally identical liner samples in the UFSC Impedance Test Rig and the NASA Langley Research Center Grazing Flow Impedance Tube (GFIT). Due to the geometrical differences between the test rigs, it is possible to consider the effect of different grazing flow profiles on the educed impedance. Impedance measurements between the two facilities show similar results in absence of grazing flow, and different results when the grazing flow is present. Results are presented with both test rigs targeted to two different conditions: (i) same centerline Mach number and; (ii) same average Mach number. Both comparisons suggest a higher acoustic resistance obtained with the UFSC Impedance Test Rig. A comparison using semiempirical predictive models was also conducted. The results suggest that the main source for the observed difference is the grazing flow profile, represented by its boundary layer displacement thickness.

I. Introduction

Acoustic liners are passive devices applied to turbofan nacelles to attenuate fan noise. A liner is commonly composed of a honeycomb structure covered with a perforate plate and backed with a rigid panel, with the liner being usually tuned to match the fundamental fan blade pass frequency (BPF). The increase in the bypass ratio of modern turbofan engines is presenting a new challenge to typical acoustic liners, in view of larger engine diameters involved. This leads to a reduction of the fan BPF, requiring the liner to have a deeper cavity. This requirement is in direct conflict with the reduced space available due to the larger engine diameter. In order to address such challenges, considerable effort is being made to design novel liner concepts that can achieve similar attenuation but with reduced dimensions. However, the proper characterization of liners in the presence of high Sound Pressure Levels (SPLs) and grazing flow, as well as the physics involved in the sound attenuation by the liner, remain topics of discussion in the community.

Typically, an acoustic liner is characterized by its acoustic impedance, which is known to depend on both liner geometry (cavity height, percentage of open area, hole diameters, etc.) and the operational condition, such as grazing flow speed and SPL [1–5]. As a consequence, the measurement of acoustic liner impedance must be carried out in conditions as close as possible to the nacelle environment. In this sense, a group of impedance eduction techniques has been proposed with the main goal of properly characterizing acoustic liners in realistic conditions. The basic approach

---

*PhD Student, Department of Mechanical Engineering, lucas.bonomo@lva.ufsc.br, Non-AIAA Member.

†MSc Student, Department of Mechanical Engineering, nicolas.quintino@lva.ufsc.br, Non-AIAA Member.

‡Associate Professor, Department of Mechanical Engineering, julio.cordioli@ufsc.br, AIAA Member.

§Assistant Professor, Dimeas Department, Corso Duca degli Abruzzi 24, francesco.avallone@polito.it, AIAA Member.

¶Senior Research Scientist, Research Directorate, Structural Acoustics Branch, AIAA Associate Fellow.

‖Research Scientist, Research Directorate, Structural Acoustics Branch, brian.m.howerton@nasa.gov, Senior Member.

**Senior Research Scientist, Research Directorate, Structural Acoustics Branch, AIAA Associate Fellow.

consists of placing an acoustic liner sample in an instrumented duct with a grazing flow superimposed by an acoustic field. The liner acoustic impedance is then educed from the measurement of the acoustic field inside the test rig.

In spite of the great number of published articles on impedance eduction techniques, few comparisons between test rigs and eduction methodologies using the same liner sample are available. Recently, the International Forum for Aviation Research (IFAR) proposed a collaboration project with this goal [6, 7]. Challenge #1 under the IFAR liner topic consisted of gathering data from multiple test rigs with simple liner configurations that could be built using 3D printing technology. However, 3D printing equipment can display large variations in precision and surface finishing, which led to some concerns regarding sample similarity in view of the differences expected during the manufacturing process [6]. Similarly, different geometries and flow generation systems of the test rigs likely resulted in different flow profiles at each rig, which were not evaluated in that study. The work of Kooi and Sarin [1] indicated that there may be a strong dependence of the liner local impedance with the flow profile over the perforate sheet.

The main goal of the present work is to provide a rigorous comparison between the impedance eduction results obtained by two different test rigs for a pair of identical 3D printed samples manufactured one after the other by the same vendor using the same equipment. The two test rigs are the impedance test rig at the Federal University of Santa Catarina (UFSC) and the NASA Langley Research Center Grazing Flow Impedance Tube (GFIT). It is expected that the fact that the same manufacturer/equipment was used to produce the samples will result in test samples that are as similar as possible, with the only difference being the overall dimension of the samples due to the different geometries of the rigs. In this sense, it is also expected that the different geometries lead to different flow profiles in the test rigs, which is also evaluated in the test campaigns. For the purpose of this comparison, tests are conducted for two different conditions: (i) same average Mach number and; (ii) same centerline Mach number. Both institutions use a direct eduction method based on Prony's algorithm to evaluate the liner impedance. Also, in order to verify any differences in the algorithms implementation used, the raw data was shared between the institutions so that each one can post-process the data obtained in the other test rig. Finally, a detailed analysis of the results is provided, including a comparison of the educed impedance with a semiempirical model of the liner impedance.

This document is organized as follows. Section II describes the impedance eduction technique used in this work; a detailed description of both test rigs is provided; also, a description of the Goodrich Semiempirical Perforate Liner Impedance Model that will be used in later analysis is presented. Section III presents the main results and discussions. Finally, the main conclusions are outlined in Section IV.

II. Experimental Setups and Methods

A. Impedance Eduction

For the purpose of this work, both test rigs can be simplified as a bidimensional duct. Assuming temporal dependence in the form of $\exp(i\omega t)$, the acoustic propagation can be modeled by the Convected Helmholtz equation, which is given by

$$\left(ik + M\frac{\partial}{\partial z}\right)^2 p - \frac{\partial^2 p}{\partial x^2} - \frac{\partial^2 p}{\partial z^2} = 0, \tag{1}$$

where p is the complex acoustic pressure, $k = \omega/c_0$ is the free-field wavenumber, ω is the angular frequency, c_0 is the speed of sound, $M = U/c_0$ is the flow Mach number and U is the flow velocity, with Cartesian coordinates x and z in the transverse and axial directions, respectively.

The solution to Eq. (1) is given by a sum of downstream and upstream acoustic propagating modes,

$$p(x, z) = \sum_{n=1}^{\infty} A_n^+ \psi_n^+(x) \exp(-i\zeta_n^+ z) + \sum_{n=1}^{\infty} A_n^- \psi_n^-(x) \exp(-i\zeta_n^- z), \tag{2}$$

where $A_n^\pm$ are the modal amplitudes, $\psi_n^\pm(x)$ are the mode shapes, $\zeta_n^\pm$ are the axial wavenumbers, n is the mode index and $+$ and $-$ denote downstream and upstream propagating waves, respectively. In the lined section of the duct, the bottom wall ($x = 0$) is lined with a wall impedance Z of length L, while the upper wall ($x = H$, where H is the duct height) is rigid. The normal component of the acoustic particle velocity vanishes in the presence of a rigid wall, such that the boundary condition is given by

$$\frac{\partial p}{\partial x} = 0, \quad \text{at } x = H. \tag{3}$$

2

For lined walls, the diffraction in the boundary layer is taken into account by means of the Ingard-Myers boundary condition [8, 9], leading to

$$\frac{\partial p}{\partial x} = \frac{Z_0}{ikZ}\left(ik + M\frac{\partial}{\partial z}\right)^2 p, \quad \text{at } x = 0, \tag{4}$$

where $Z_0 = \rho_0 c_0$ is the air characteristic impedance and ρ_0 is the air density. These boundary conditions applied to Eq. (2) lead to the eigenvalue problem

$$\alpha_n \tan(\alpha_n H) - \frac{Z_0}{ikZ}(ik - iM\zeta_n)^2 = 0, \tag{5}$$

where α_n are the transverse wavenumbers, and the dispersion relation is given by

$$\alpha_n^2 = (k - M\zeta_n)^2 - \zeta_n^2. \tag{6}$$

Hence, once the axial wavenumber is known, it is straightforward to calculate the liner impedance from solving the system of equations obtained from Eqs. (5) and (6).

In order to extract the axial wavenumber, one can use Prony-like algorithms to fit a sum of damped complex exponentials to the measured acoustic pressure at uniformly spaced locations[10]. In this case, the acoustic pressure at the flush-mounted microphones at the wall opposite to the liner sample is given by

$$p_j = \sum_{n=1}^{\infty} A_n \exp(-i\zeta_{n,j}\Delta z)^j + w_j \quad \text{for } j = 0, ..., \mathcal{M} - 1, \tag{7}$$

where p_j is the pressure at the j-th microphone, Δz is the distance between two consecutive microphones, w_j is the measurement noise, and $\mathcal{M}$ is the number of microphones.

One main issue of using the original Prony's algorithm, as proposed by Jing et al. [10], is its poor performance in the presence of noise w_j [11]. As an alternative, the Kumaresan and Tufts (KT) algorithm [11], has been successfully applied [5, 12], providing lower uncertainty levels by selecting a reduced number of wavenumbers (propagating modes)[13]. In this work, the KT algorithm will be used by both teams to extract the axial wavenumbers from measured acoustic fields, but with different strategies to select the wavenumbers.

The UFSC team selects the least attenuated mode, which is normally associated with the most energetic mode [13]. On the other side, the NASA Langley team takes advantage of the higher number of microphones, which allows a higher number of extracted wavenumbers, and initially selects the 5 lowest order modes. An interactive process is than applied that follows the sequence: (i) computes the impedance from each mode, (ii) uses that impedance to compute the sound field, and (iii) selects the impedance/mode that minimizes the difference between computed and experimental sound field. More details of the KT algorithm implementation can be found in the Appendix.

B. UFSC Liner Impedance Test Rig

The UFSC Liner Impedance Test Rig is a grazing flow acoustic impedance facility located at the Laboratory of Vibration and Acoustics of the Federal University of Santa Catarina, Brazil. A 3-dimensional schematic view of the test rig is shown in Fig. 1. The test rig is composed of modular rectangular cross-sectioned $40\text{x}100\,\text{mm}^2$ ducts. Quasianechoic terminations at the test rig inlet and outlet minimize acoustic reflections. Eight Beyma CP-855nD compression drivers are distributed both upstream and downstream of the liner test sample holder, in order to generate sound fields up to 150 dB propagating both toward and against the flow. Grazing flow is supplied by an external compressed air system, which is able to sustain a cross-section averaged flow up to Mach 0.7. A KIMO CP-115 differential pressure transmitter is connected to a 2 mm diameter pitot tube located at the test rig inlet. This pitot tube is used to control the flow speed by using a precalibrated factor. Temperature is monitored with a KIMO TM-110 temperature transmitter at the test rig inlet.

An array of eight equally-spaced flush-mounted B&K DeltaTron 4944 1/4" pressure field microphones is located on the wall opposite to the liner section for the impedance eduction. Signals are recorded with a National Instruments PXIe-4499 daq module at a sampling rate of 25.6 kHz. Measurements are performed using the excitation signal as reference for cross-spectrum estimation using Welch's method with 30 averages of 25 600 samples with 75 % overlap. In-house Python3 codes are used for all hardware control, signal processing and post-processing the data.
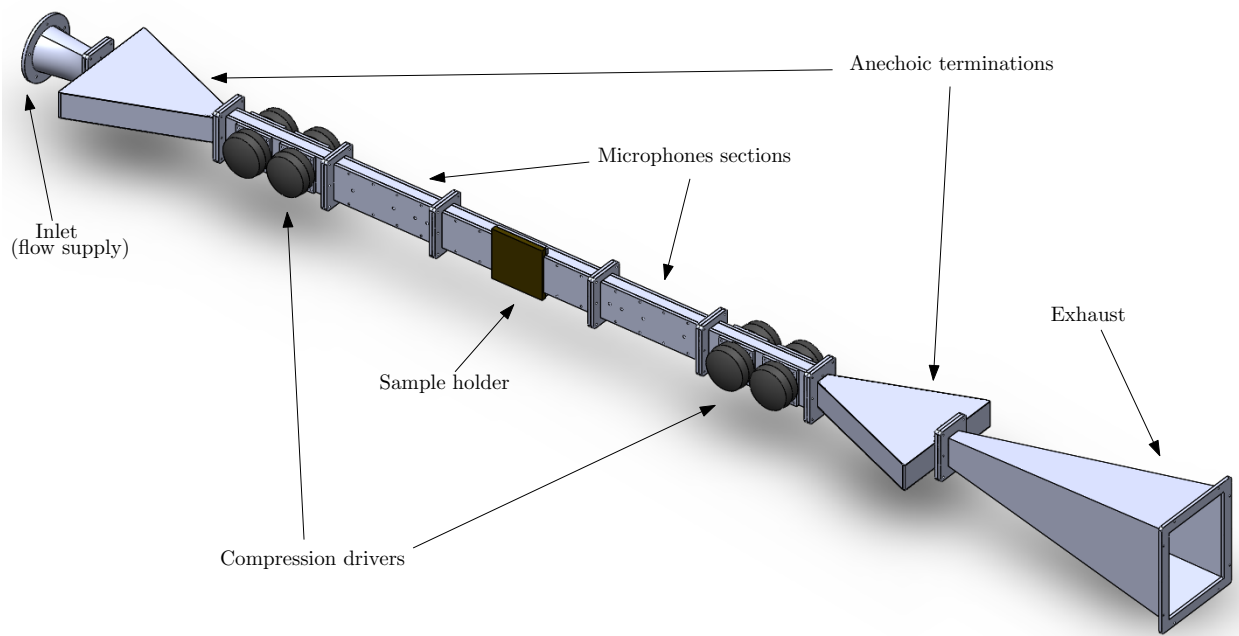
Fig. 1   Schematic representation of the UFSC Liner Impedance Test Rig.

C. GFIT

The NASA Langley GFIT facility is used to measure the acoustic characteristics of noise reduction treatments (acoustic liners) for aircraft jet engine nacelles and nozzles. The facility is a wind tunnel with a 50.8 mm by 63.5 mm rectangular cross section and can be seen schematically in Fig. 2. The flow path consists of a straight duct with an upstream acoustic source section using 12 drivers, interchangeable lengths of blank duct, a test section where the liner sample is held along the upper wall of the duct and an array of 95 measurement microphones leading to a 6-driver downstream source section. Near-anechoic terminating diffusers are employed at each end of the duct to control reflections and reduce overall flow noise. The source sections can generate sound pressure levels (SPL) up to 150 dB for the frequency range between 400 and 3000 Hz. In the current work, sine swept excitation is used to cover the desired frequency range. To generate the desired flow conditions, pressurized and heated air is supplied to the inlet of the GFIT while a vacuum system is employed at the duct exit to evacuate air from the tube. With this arrangement, static pressure at the test section can be held to near ambient conditions at all flow velocities with constant total temperature. Grazing flow velocities from 0 to Mach 0.6 are available with such an arrangement.
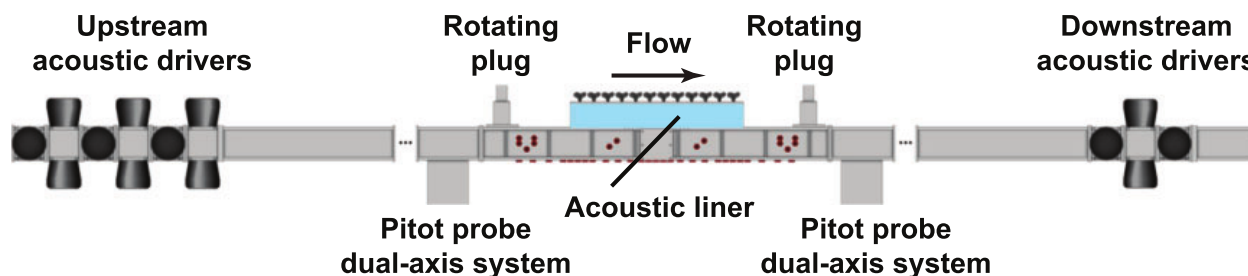

Fig. 2   Schematic representation of the NASA Langley Research Center Grazing Flow Impedance Tube (GFIT).

D. Goodrich Semiempirical Perforate Liner Impedance Model

The Goodrich semiempirical perforate liner impedance model used in this work was presented by Yu et al. [14]. The basic equation of the model is given by

$$Z = Z_{\text{of}} + S_r u_0 + R_{\text{cm}} + \mathrm{i} \left(S_{\text{m}} u_0 - \cot(kh)\right), \tag{8}$$

where Z_{of} is the perforate plate impedance, S_r is the nonlinear resistance slope, u_0 is the root-mean-squared acoustic particle velocity, R_{cm} the normalized grazing flow induced acoustic resistance, S_{m} the nonlinear mass reactance and h the liner cavity height.

The perforate plate impedance is given by

$$Z_{\text{of}} = \mathrm{i}\omega \frac{(t + \varepsilon d) F(k_s d/2)}{c_0 \sigma}, \tag{9}$$

where t is the facesheet thickness, d is the perforate plate hole diameter, σ the percentage of open area, $F(k_s d/2)$ the cross-section averaged hole velocity profile from Crandall's solution and

$$\varepsilon d = \frac{d(1 - 0.7\sqrt{\sigma})}{1 + 305 M^3}, \tag{10}$$

is the effective mass end correction. The cross-section-averaged hole velocity profile is defined as

$$F(k_s d/2) = 1 - \frac{2 J_1(k_s d/2)}{k_s (d/2) J_0(k_s d/2)}, \tag{11}$$

where J_0 and J_1 are zero- and first-order Bessel functions and

$$k_s^2 = -\mathrm{i}\frac{\omega \rho}{\mu}, \tag{12}$$

is the wavenumber of a viscous Stokes wave, where ρ is the air density and μ the air viscosity. The nonlinear resistance slope is given by

$$S_r = 1.336541 \left(\frac{1 - \sigma^2}{2 C_d^2 \sigma^2}\right), \tag{13}$$

where C_d is the discharge coefficient, which for $t/d \leq 1$ is given by

$$C_d = 0.80695 \sqrt{\frac{\sigma^{0.1}}{\exp(-0.5072 t/d)}}. \tag{14}$$

The normalized grazing flow induced acoustic resistance is

$$R_{\text{cm}} = \frac{M}{\sigma \left(2 + 1.256\dfrac{\delta^*}{d}\right)}, \tag{15}$$

where δ^* is the flow profile boundary layer displacement thickness. Finally, the nonlinear mass reactance is

$$S_{\text{m}} = -0.0000207 \frac{k}{\sigma^2}. \tag{16}$$

E. Test Matrix and Liner Samples

For the purpose of this work, two liner samples were manufactured via stereolithography additive manufacturing. The liner sample was designed as an array of individual $9.9 \times 9.9\,\text{mm}^2$ square chambers, with 8 holes with a diameter $d = 0.99\,\text{mm}$, resulting in a single chamber percentage of open area of 6.3 %. The facesheet thickness is $t = 0.635\,\text{mm}$. The cell walls are 2.54 mm (0.1") thick, resulting in a overall percentage of open area of 4.2 %. Each sample was arranged to fit the different sample holders from the test rigs. The UFSC sample consists of an array of 8×33 cells, while the NASA sample is 4×44. Since no backplate was added in the 3D model, a 6.35 mm (1/4") thick aluminum plate was used as the liner sample backplate. The UFSC sample can be see in Fig. 3.

Tests were conducted with two centerline Mach numbers, $M_{\text{center}} = 0.3$ and 0.5, for the average Mach number $M_{\text{avg}} = 0.3$ and in absence of flow. A stepped pure tone excitation was used, in a frequency range from 500 Hz to 2500 Hz with 100 Hz steps. The sound pressure level was set 130 dB, with the acoustic source located upstream or downstream (one at a time) of the liner.
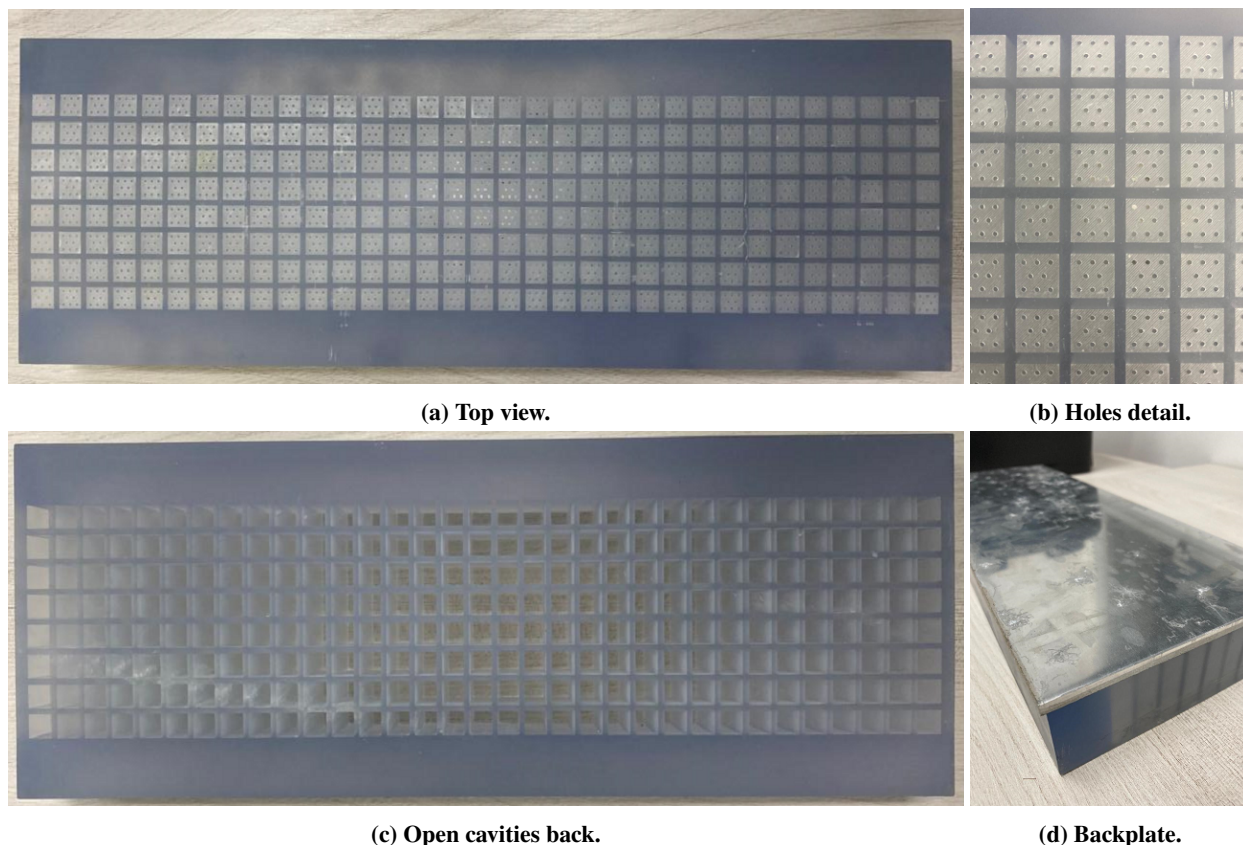
5

(a) Top view.

(b) Holes detail.

(c) Open cavities back.

(d) Backplate.

Fig. 3   Pictures from UFSC test sample.

III. Results and Discussion

A. Flow Profiles

This section presents the flow profiles experimentally measured for both test rigs with a centerline Mach number 0.3. The description for the NASA measurements can be found in Jones et al. [15]. For the UFSC flow profile, the measurements were performed with a 3 mm diameter pitot tube at the liner sample upstream edge position. Measurements were done with the help of a micrometer linear table with 1 mm step. The flow profiles are presented in Fig. 4. The boundary layer displacement thicknesses (BLDT, δ^*) for both test rigs were evaluated from the measured data and the approximated values are $\delta^*_{\text{UFSC}} = 1.02$ mm and $\delta^*_{\text{GFIT}} = 2.60$ mm.

B. Acoustic Results

In this section, the impedances educed with the KT algorithm in both test rigs are compared. The experimental results are also compared with the prediction from the Goodrich semiempirical model for each test rig. In the first approach, the test rigs were set to match the same maximum Mach number (centerline Mach number) in the cross-section, which provided slightly different average Mach numbers.

The results obtained with both tests rigs at 130 dB in the absence of mean flow are presented in Fig. 5. Overall, a very good agreement is observed, especially in the frequency range of higher acoustic attenuation, where the experimental uncertainties are expected to be low [13]. The discrepancy in the resistance slope observed in lower frequencies may be explained by the low attenuation level and/or reduced liner length/wavelength ratio [16]. This agreement with no flow gives confidence in the manufacturing process and the samples' similarity, allowing further comparisons with grazing flow.

Figures 6a and 6b show the results obtained with both test rigs at 130 dB and both propagation directions for centerline Mach numbers of 0.3 and 0.5, respectively. The results follow the expected pattern, i.e., the resistance
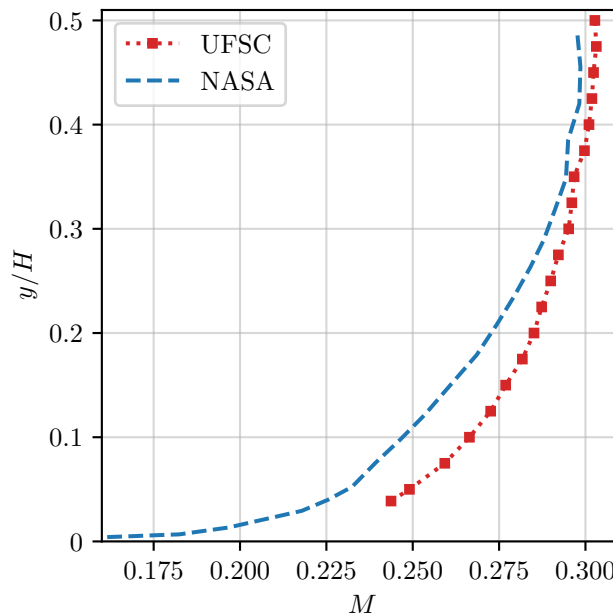
6

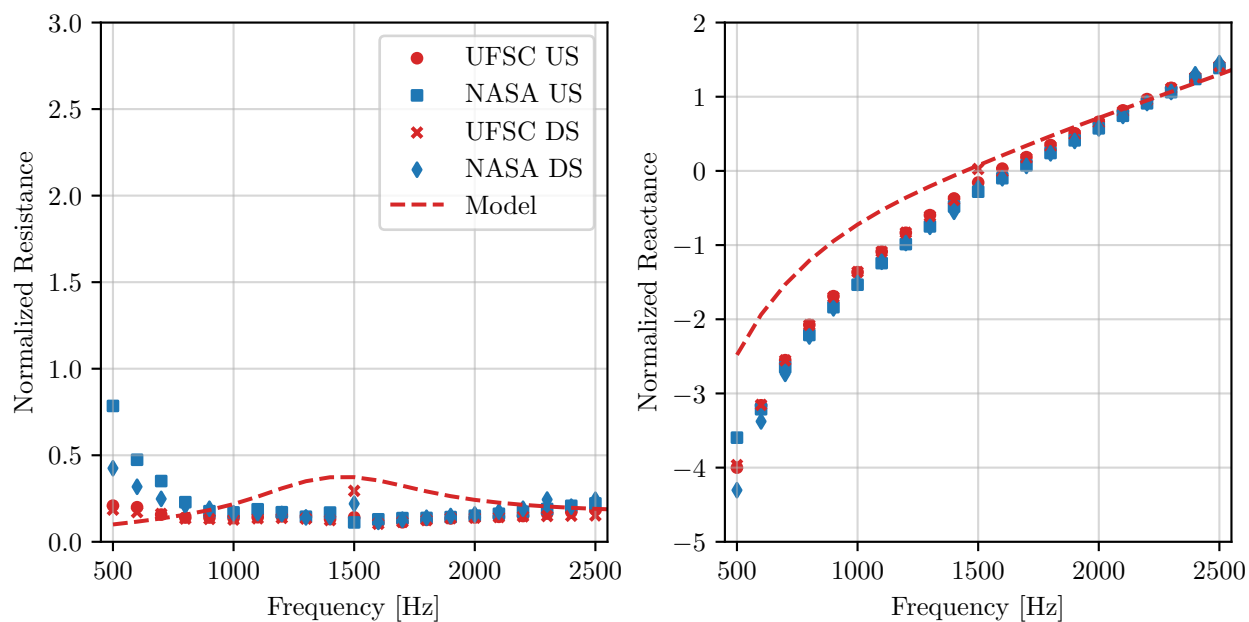**Fig. 4   Flow profiles obtained for centerline Mach number 0.3.**

Fig. 5   Educed impedances in absence of flow and at 130 dB. US: Upstream source (downstream propagation); DS: Downstream source (upstream propagation).

increases with higher grazing flow Mach numbers. Also, the results obtained with both test rigs exhibit the differences reported in the literature between upstream and downstream acoustic source configurations. These differences are still under debate in the community, whether as a failure of the Ingard-Myers boundary condition or an inherent part of liner physics [5, 17]. However, significant differences can be observed between the results obtained from each test rigs. In spite of a very good agreement observed in the educed reactance, the acoustic resistance measured within the UFSC facility is consistently higher than the one measured in the NASA GFIT.

As mentioned earlier, the flow profile is expected to affect the liner resistance [1]. In order to verify the possible
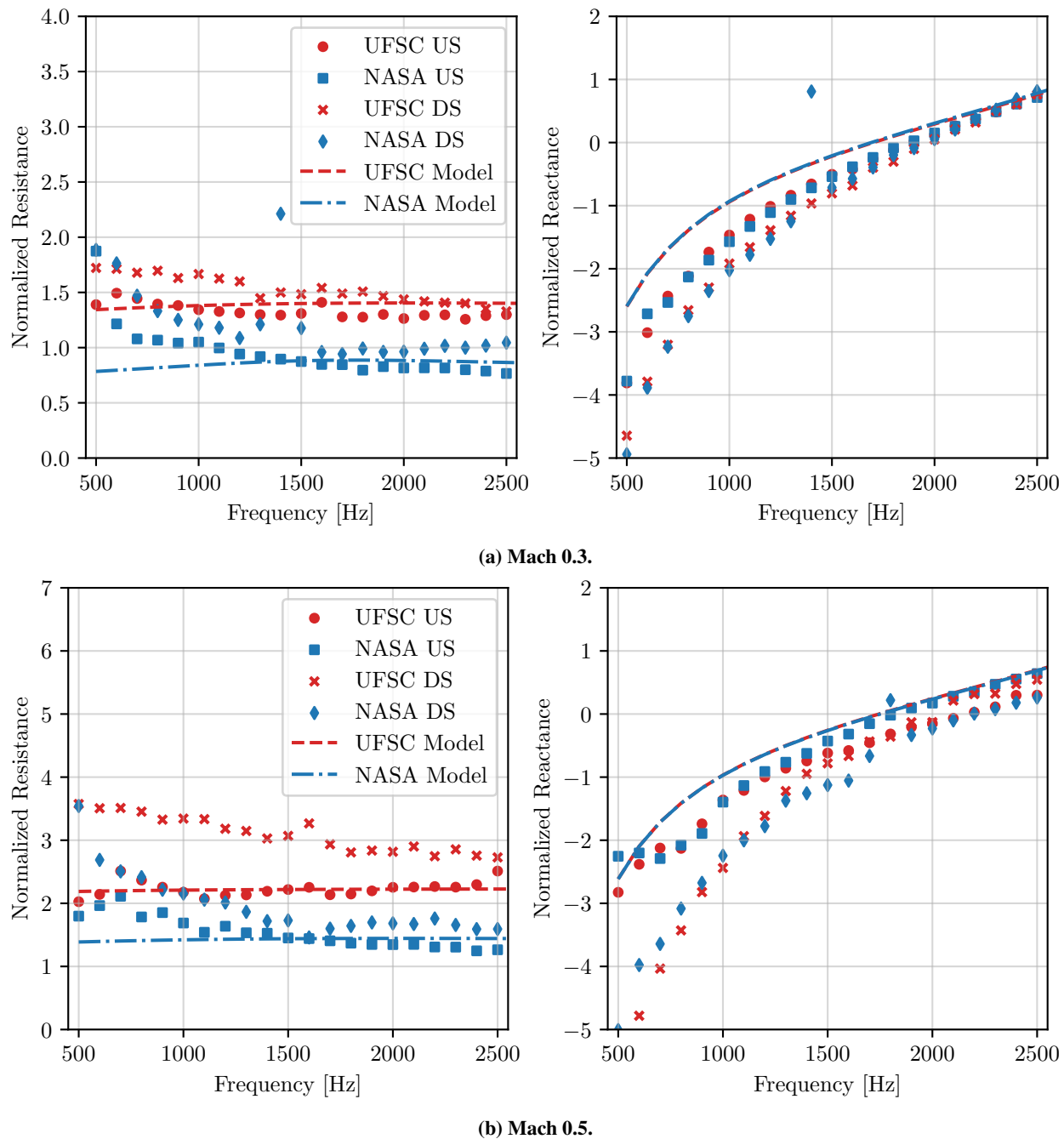
(a) Mach 0.3.

(b) Mach 0.5.

Fig. 6   Educed impedances with centerline Mach number 0.3 and 0.5 and at 130 dB. US: Upstream source (downstream propagation); DS: Downstream source (upstream propagation).

impact of the different flow profiles measured at each test rig, the results obtained with both the UFSC Test Rig and the NASA GFIT are compared to the impedance prediction obtained with the semiempirical model presented in Section II.D, with the only difference being the boundary layer displacement thickness δ^* measured at each test rig. The semiempirical model used was originally developed by best-fitting the model to data they obtained with the in-situ technique (for details of the in situ technique, see Ref. [16]), hence some differences between the educed results and the semiempirical modes are expected. This is quite clear at the low frequency range where results from the in situ technique do not generally display the resistance slope observed in eduction methods [16]. Nevertheless, the semiempirical model prediction

8

captures really well the difference observed in the resistance between results from each test rig, suggesting that the flow profile plays an important role in the eduction process.

One may question if the differences observed between the results from each test rig are due to errors in the average Mach number between the test rigs rather than the flow profile. Indeed, due to the difference in the flow profile, matching the centerline Mach number does not imply the same average Mach number. In order to investigate the sensitivity of the semiempirical model to both flow profile (in the form of the boundary layer displacement thickness, δ^*) and the average Mach number, a parametric analysis was conducted. A range of average Mach number and δ^* from the two test rigs was evaluated, and the results obtained with the semiempirical model are presented in Fig. 7. Results from the parametric analysis show that the dominant effect is indeed the flow profile, while the difference due to the average Mach number is much smaller.
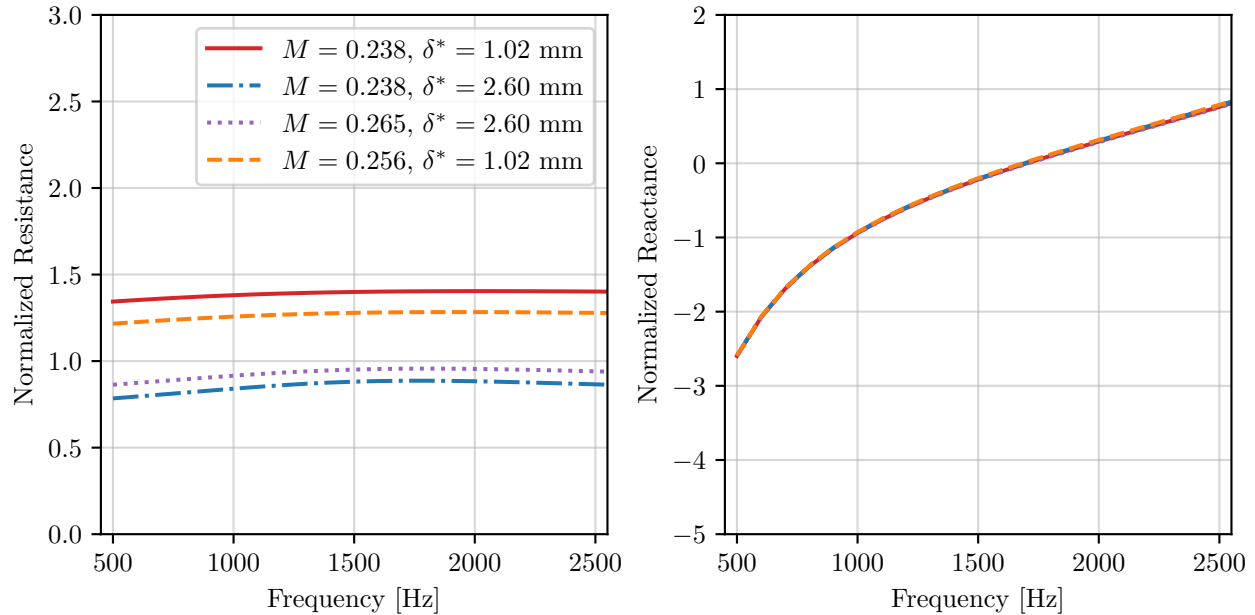

Fig. 7   Parametric analysis performed with the Goodrich semiempirical model. $M = 0.265$ and $\delta^* = 1.02$ mm corresponds to UFSC data and $M = 0.238$ and $\delta^* = 2.60$ mm to GFIT flow profile measurements.

In order to validate the parametric analysis, a new set of tests were conducted at the NASA GFIT test rig. In this case, the flow velocity was targeted to match the same average Mach number as the one observed at the UFSC test rig, $M_{\text{avg}} = 0.265$. The new comparison is presented in Fig. 8. It can be seen that results display the very similar discrepancy to that observed in Figs. 6a and 7 for the case with the same centerline Mach number. This result confirms that the flow profile plays a relevant role in the impedance eduction and must not be neglected in further comparisons.

Different eduction methods may lead to small differences in the educed impedance even with data collected within the same test rig [16]. In this sense, an analysis is required to verify if the eduction algorithms applied by the teams led to any key difference in the previous results. For this purpose, it was proposed that both teams share with each other the raw acoustic pressure and all other parameters necessary for the eduction process (Mach, temperature, detailed geometric dimensions of the test rig, etc.) and then compare the educed acoustic impedances. For this work, NASA data are going to be used, since the longer sample and higher number of microphones available must provide lower uncertainties with Prony-like methods [13]. The comparison was performed with both acoustic source locations and centerline Mach numbers of 0.0 (no flow), 0.3 and 0.5. The results obtained are presented in Figs. 9a and 9b for upstream and downstream acoustic sources, respectively.

As expected, the comparison of educed impedances using the same dataset presented an almost perfect match. Small differences are observed with higher Mach numbers and downstream source, which may be explained by the mode selection process that can lead to some differences in the educed impedance [13]. This final analysis corroborates that the previous observed differences may come from the different flow profiles of the test rigs.
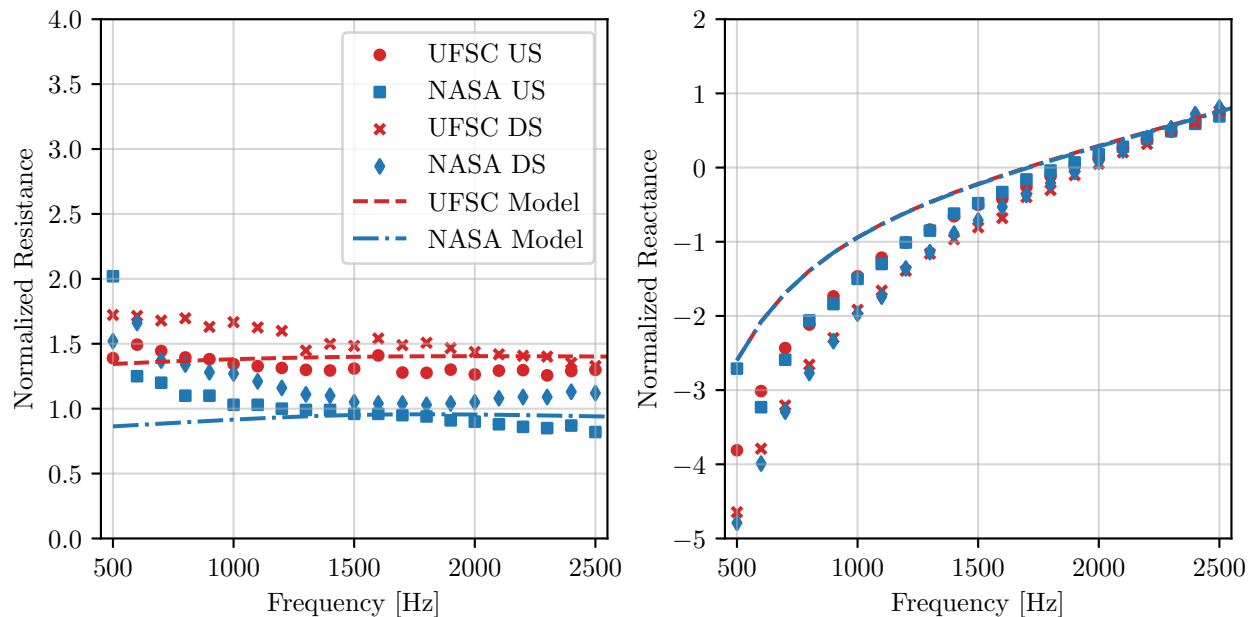
Fig. 8   Educed impedances with same mean flow Mach number 0.265 and at 130 dB in both test rigs. US: Upstream source (downstream propagation); DS: Downstream source (upstream propagation).

IV. Concluding Remarks

This paper presented a comparison of impedance results obtained using two impedance eduction test rigs for the same liner. Two liner samples were manufactured with equal cavity geometries by the same 3D printing equipment for both test rigs, in order to reduce errors induced by the manufacturing process. One sample was taken by the NASA Langley acoustic liner team to be tested within the GFIT, and the other was sent to the UFSC team to be tested within the UFSC Liner Test Rig. The samples were first tested with both test rigs targeted to match the same centerline Mach number. Results obtained by UFSC presented acoustic resistances significantly higher then those observed by the NASA Langley team in the presence of grazing flow. A semiempirical model was used to identify the key parameter affecting the results, and the flow profile boundary layer displacement thickness, δ^*, was pointed to as the main source of discrepancies. The tests were conducted again so that the average Mach number at the GFIT was targeted to match the average Mach number of the UFSC test rig. The new set of results presented the same discrepancy pattern, which suggests that the higher acoustic resistances may come from the different flow profiles inside the test rigs. As a final remark, the raw data obtained by NASA Langley team were shared with the UFSC team to a cross-comparison of eduction algorithms. No significant difference was observed in the impedances educed using the two different algorithms, corroborating the hypothesis that different flow profiles is the cause of the discrepancies in the impedance results.

V. Appendix

A. KT Algorithm

The basic idea of Prony-like methods consists of fitting a sum of damped complex exponentials to the measured acoustic pressure field at uniformly spaced locations. For this purpose, an array of microphones is flush-mounted at the wall opposite to the liner sample, so

$$p_j = \sum_{n=1}^{\infty} A_n \exp(-\mathrm{i}\zeta_{n,j}\Delta z)^j + w_j \quad \text{for } j = 0, ..., \mathcal{M} - 1, \tag{7}$$

where p_j is the pressure at the j-th microphone, Δz is the distance between two consecutive microphones, w_j is the measurement noise, and $\mathcal{M}$ is the number of microphones. Initially it is assumed that the acoustic field in the lined section is dominated by $\mathcal{N}$ modes. Also, assuming a noiseless signal, $w_j = 0$, and choosing a convenient model order

10

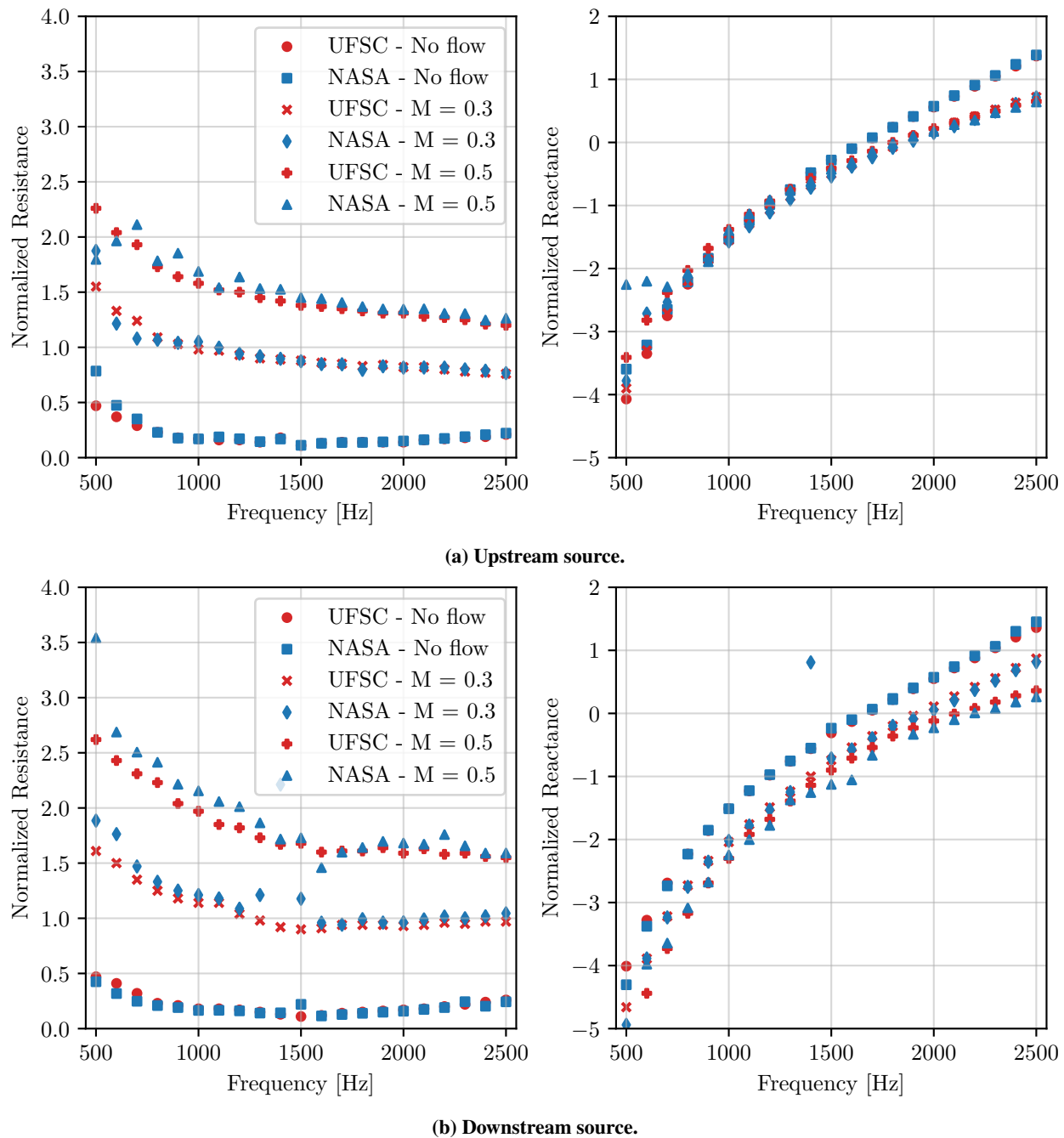**(a) Upstream source.**

(b) Downstream source.

Fig. 9 Educed impedances with NASA data post-processed by UFSC and NASA for the three centerline Mach numbers and at 130 dB.

$\mathcal{L}$, which satisfies $\mathcal{N} \leq \mathcal{L} \leq \mathcal{M} - \mathcal{N}$, Eq. (7) becomes

$$p_{j+r} = \sum_{n=1}^{\mathcal{L}} A_n V_n^{(j+r)} \quad \text{for } r = 0, ..., \mathcal{M} - \mathcal{L} - 1, \tag{17}$$

where $V_n^{(j+r)} = \exp(-\mathrm{i}\zeta_{n,j}\Delta z)$, for later convenience.

11

If a_j are the coefficients of the characteristic polynomial,

$$\sum_{j=0}^{\mathcal{L}} a_j V^i = 0, \tag{18}$$

then it is possible to show that

$$\sum_{j=0}^{\mathcal{L}} a_j p_{j+r} = 0, \tag{19}$$

which in the matrix form is given by

$$\mathbf{Ha} = -\mathbf{b}, \tag{20}$$

where

$$\mathbf{H} = \begin{bmatrix} p_1 & p_2 & \cdots & p_{\mathcal{L}} \\ p_2 & p_3 & \cdots & p_{\mathcal{L}+1} \\ \vdots & \vdots & \ddots & \vdots \\ p_{\mathcal{M}-\mathcal{L}} & p_{\mathcal{M}-\mathcal{L}+1} & \cdots & p_{\mathcal{M}-1} \end{bmatrix}, \ \mathbf{a} = \begin{bmatrix} a_1 \\ a_2 \\ \vdots \\ a_{\mathcal{L}} \end{bmatrix}, \ \mathbf{b} = \begin{bmatrix} p_0 \\ p_1 \\ \vdots \\ p_{\mathcal{M}-\mathcal{L}-1} \end{bmatrix}, \tag{21}$$

which is solved for the polynomial coefficients $\mathbf{a}$ in a least square sense. From that, the system zeros V_n are given by the roots of Eq. (18), with $a_0 = 1$. Finally, the axial wavenumbers are computed from

$$\zeta_n = \frac{\ln(V_n)}{-\mathrm{i}\Delta z}. \tag{22}$$

The condition where a model order $\mathcal{L} = \mathcal{M}/2$ was selected corresponds to the original Prony's method. One main issue of Prony's algorithm is its poor performance in the presence of noise [11]. Kumaresan and Tufts [11] proposed the use of singular value decomposition (SVD) to better estimate the coefficients of the polynomial, Eq. (18), hereinafter labeled as the KT algorithm. The main difference consists in identifying and removing spurious poles by performing an SVD on matrix $\mathbf{H}$,

$$\mathbf{H} = \mathbf{USV}^H, \tag{23}$$

where $\mathbf{U}$ and $\mathbf{V}$ are unitary matrices, $\mathbf{S}$ contains the σ_j singular values of $\mathbf{H}$ on the main diagonal, and $\mathbf{V}^H$ denotes the conjugate transpose of $\mathbf{V}$. The reduced rank approximation of $\mathbf{H}$ is then given by

$$\mathbf{H}_Q = \mathbf{US}_Q\mathbf{V}^H, \tag{24}$$

where only the first Q singular values are considered, such that $\sigma_j = 0$ for $j > Q$. Therefore, the coefficients of the polynomial can be found by

$$\mathbf{H}_Q\mathbf{a} = -\mathbf{b}. \tag{25}$$

The truncated matrix leads to spurious poles inside the unitary circle, which allows the identification of physical poles [11]. Watson et al. [12] used this criterion to select the pole corresponding to the least attenuated mode.

The choice of Q is not trivial since this parameter may depend on frequency, test sample and flow velocity. In this work, the same methodology presented by Weng et al. [18] is used, which consists of a criterion based on the minimum description length (MDL), given by,

$$\mathrm{MDL}_m = -(\mathcal{L} - m)\mathcal{M} \ln\left(\frac{\prod_{j=m+1}^{\mathcal{L}} \sigma_j^{1/(\mathcal{L}-m)}}{\frac{1}{\mathcal{L}-m} \sum_{j=m+1}^{\mathcal{L}} \sigma_j}\right) + \frac{m(2\mathcal{L} - m)}{2} \ln(\mathcal{M}), \quad \text{for } m = 1, ..., \mathcal{L}. \tag{26}$$

The index m of the minimum MDL_m corresponds to the number of modes Q to be used in reduced rank approximation of $\mathbf{H}$. Specifically for the Kumaresan and Tufts method, we consider a different model order $\mathcal{L}$, which is now given by $\mathcal{L} = 3\mathcal{M}/8$, as proposed by Renou and Aurégan [5]. Such a procedure transforms Eq. (20) into an overdetermined system of equations, which should also increase the accuracy of the method. Finally, a process to select one of the educed wavenumbers is required. Each team uses a different process, as described in Section. II.A.

Acknowledgments

References

[1] Kooi, J., and Sarin, S., "An experimental study of the acoustic impedance of Helmholtz resonator arrays under a turbulent boundary layer," *7th Aeroacoustics Conference*, American Institute of Aeronautics and Astronautics, AIAA Paper 1981-1998, 1981. https://doi.org/10.2514/6.1981-1998.

[2] Jones, M., Tracy, M., Watson, W., and Parrott, T., "Effects of Liner Geometry on Acoustic Impedance," *8th AIAA/CEAS Aeroacoustics Conference & Exhibit*, American Institute of Aeronautics and Astronautics, AIAA Paper 2002-2446, Breckenridge, Colorado, 2002. https://doi.org/10.2514/6.2002-2446.

[3] Murray, P., Ferrante, P., and Scofano, A., "Manufacturing Process and Boundary Layer Influences on Perforate Liner Impedance," *11th AIAA/CEAS Aeroacoustics Conference*, American Institute of Aeronautics and Astronautics, AIAA Paper 2005-2849, Monterey, California, 2005. https://doi.org/10.2514/6.2005-2849.

[4] Murray, P., and Astley, R. J., "Development of a single degree of freedom perforate impedance model under grazing flow and high SPL," *18th AIAA/CEAS Aeroacoustics Conference (33rd AIAA Aeroacoustics Conference)*, American Institute of Aeronautics and Astronautics, AIAA Paper 2012-2294, Colorado Springs, Colorado, 2012. https://doi.org/10.2514/6.2012-2294.

[5] Renou, Y., and Aurégan, Y., "Failure of the Ingard–Myers boundary condition for a lined duct: An experimental investigation," *The Journal of the Acoustical Society of America*, Vol. 130, No. 1, 2011, pp. 52–60. https://doi.org/10.1121/1.3586789.

[6] Bake, F., Burgmayer, R., Schulz, A., Knobloch, K., Enghardt, L., and Jones, M. G., "IFAR liner benchmark challenge #1 – DLR impedance eduction of uniform and axially segmented liners and comparison with NASA results," *International Journal of Aeroacoustics*, Vol. 20, 2021, pp. 478–496. https://doi.org/10.1177/1475472X211023844/ASSET/IMAGES/LARGE/10.1177_1475472X211023844-FIG2.JPEG.

[7] Jones, M. G., Nark, D. M., and Howerton, B. M., "Overview of Liner Activities in Support of the International Forum for Aviation Research," *25 AIAA/CEAS Aeroacoustics 2022 Conference*, American Institute of Aeronautics and Astronautics, AIAA Paper 2019-2599, 2019. https://doi.org/10.2514/6.2019-2599.

[8] Ingard, U., "Influence of Fluid Motion Past a Plane Boundary on Sound Reflection, Absorption, and Transmission," *The Journal of the Acoustical Society of America*, Vol. 31, No. 7, 1959, pp. 1035–1036. https://doi.org/10.1121/1.1907805.

[9] Myers, M., "On the acoustic boundary condition in the presence of flow," *Journal of Sound and Vibration*, Vol. 71, No. 3, 1980, pp. 429 – 434. https://doi.org/10.1016/0022-460X(80)90424-1.

[10] Jing, X., Peng, S., and Sun, X., "A straightforward method for wall impedance eduction in a flow duct," *The Journal of the Acoustical Society of America*, Vol. 124, No. 1, 2008, pp. 227–234. https://doi.org/10.1121/1.2932256.

[11] Kumaresan, R., and Tufts, D., "Estimating the parameters of exponentially damped sinusoids and pole-zero modeling in noise," *IEEE Transactions on Acoustics, Speech, and Signal Processing*, Vol. 30, No. 6, 1982, pp. 833–840. https://doi.org/10.1109/TASSP.1982.1163974.

[12] Watson, W. R., Carpenter, M. H., and Jones, M. G., "Performance of Kumaresan and Tufts algorithm in liner impedance eduction with flow," *AIAA Journal*, Vol. 53, No. 4, 2015, pp. 1091–1102. https://doi.org/10.2514/1.J053705.

[13] Bonomo, L. A., Spillere, A. M., and Cordioli, J. A., "Parametric Uncertainty Analysis for Impedance Eduction Based on Prony's Method," *AIAA Journal*, Vol. 58, 2020, pp. 3625–3638. https://doi.org/10.2514/1.J059071.

[14] Yu, J., Ruiz, M., and Kwan, H. W., "Validation of Goodrich perforate liner impedance model using NASA langley test data," *14th AIAA/CEAS Aeroacoustics Conference (29th AIAA Aeroacoustics Conference)*, American Institute of Aeronautics and Astronautics, AIAA Paper 2008-2930, 2008. https://doi.org/10.2514/6.2008-2930.

[15] Jones, M. G., Watson, W. R., and Nark, D. M., "Effects of Flow Profile on Educed Acoustic Liner Impedance," *16 AIAA/CEAS Aeroacoustics 2022 Conference*, American Institute of Aeronautics and Astronautics, AIAA Paper 2010-3763, 2010. https://doi.org/10.2514/6.2010-3763.

[16] Bonomo, L. A., Quintino, N. T., Spillere, A. M., Cordioli, J. A., and Murray, P. B., "A Comparison of In-Situ and Impedance Eduction Experimental Techniques for Acoustic Liners with Grazing Flow and High SPL," *28th AIAA/CEAS Aeroacoustics 2022 Conference*, American Institute of Aeronautics and Astronautics, AIAA Paper 2022-2998, Southampton, UK, 2022. https://doi.org/10.2514/6.2022-2998.

[17] Spillere, A. M. N., Bonomo, L. A., Cordioli, J. A., and Brambley, E. J., "Experimentally testing impedance boundary conditions for acoustic liners with flow: Beyond upstream and downstream," *Journal of Sound and Vibration*, Vol. 489, 2020, p. 115676. https://doi.org/10.1016/J.JSV.2020.115676.

[18] Weng, C., Schulz, A., Ronneberger, D., Enghardt, L., and Bake, F., "Flow and Viscous Effects on Impedance Eduction," *AIAA Journal*, Vol. 56, No. 3, 2018, pp. 1118–1132. https://doi.org/10.2514/1.J055838.